Journal of Advanced Ceramics
2018, **7**(4): 307–316
https://doi.org/10.1007/s40145-018-0280-6

ISSN 2226-4108
CN 10-1154/TQ

Research Article

A study of morphological properties of SiO_2 aerogels obtained at different temperatures

Jin-jun LIAO[a], Peng-zhao GAO[a,*], Lin XU[b], Jian FENG[b]

[a]*College of Materials Science and Engineering*, *Hunan University*, *Changsha 410082*, *China*
[b]*Key Laboratory of New Ceramic Fibers and Composites*, *National University of Defense Technology*, *Changsha 410082*, *China*

Received: March 3, 2018; Revised: May 2, 2018; Accepted: May 2, 2018
© The Author(s) 2018. This article is published with open access at Springerlink.com

Abstract: In this paper, temperature dependence of nanoporous framework evolution process and variety of pore properties (pore volume, specific surface area (BET), and pore size) of SiO_2 aerogels were characterized by FTIR, XPS, XRD, SEM, TEM, BET, BJH, etc. Results show that SiO_2 aerogels treated at different temperatures all possess amorphous structure. With the increase of treated temperatures, BET values of SiO_2 aerogels increase initially and then decrease, and it reaches the maximum value of 882.81 m^2/g when treated at 600 ℃ for 2 h due to the addition of the nanopores and shrinkage skeleton of SiO_2 aerogels. Higher temperatures may result in a framework transformation and particle growth; both factors could reduce the BET values of the aerogels. Nanoporous skeleton of SiO_2 aerogels at room temperatures is composed of tetrahedron with a pore size of about 22.28 nm. Higher treated temperatures result in an increase of octahedron amount in nanoporous framework and a decrease of pore size. When treated at 1000 ℃, an approximate dense SiO_2 bulk via the framework collapse and particle growth is obtained. These varieties are derived from the formed extra bonds of Si–O–Si, higher local stress, and liquid phase between particles during heat treatment process.

Keywords: silica aerogel; temperature dependence; nanoporous framework evolution; pore properties

1 Introduction

Silica (SiO_2) aerogels show potential applications in the fields of catalysis, environmental protection, thermal insulation materials, electrical, optics, acoustic impedance materials, low bulk density materials (~0.03 g/cm^3), nanoporous materials, high porosity (> 90 %), high surface area (500–1000 m^2/g) and low thermal conductivity (0.005 W/(m·K)) materials [1–5], due to the nanoparticles and special nanoporous framework. While the special skeleton of aerogel may be destroyed and nanoparticles may grow up at higher temperatures, both can acutely reduce the density and thermal properties of SiO_2 aerogel [6]. Many researches concentrated on strengthening the thermal stability and strength of the aerogel via the preparation of hybrid aerogels [7–11]. Kim *et al.* [9] synthesized a glass fiber/silica aerogel, which possessed bigger pore size and specific surface area than aerogel composites made of only colloidal silica. Wu *et al.* [10] fabricated aerogel composites using a multilayer aligned glass

* Corresponding author.
E-mail: gaopengzhao7602@hnu.edu.cn

fiber as reinforcer, which owned a low thermal conductivity of 0.022–0.028 W/(m·K) and compressive strength of 1.71–3.70 MPa. Fenech *et al.* [11] prepared ZrO_2/Y_2O_3 aerogels with BET surface area of 159 and 26 m^2/g after heat treatment at 550 and 1000 ℃ respectively.

It is known that the performance of a porous material depends on the pore size and framework structure [12], and these will vary at high temperatures. There are a limited number of studies that report the relationship between the nanoporous framework formation and particle growth process with the pore properties of SiO_2 aerogels obtained at different temperatures [16]. Zhou *et al.* [13] studied the framework structure of aerogels with two different granular sizes of 5 and 20 nm. They found that the small pores collapsed while the large pores expended after calcination at high temperatures. Huang *et al.* investigated the structural changes of silica aerogels in the 950–1200 ℃ temperature range. Their results showed that the process consists of three steps [14,15].

The aim of this work is to study the process of SiO_2 aerogel nanoporous framework formation and particle growth at different temperatures with a series of physicochemical methods, among others with FTIR, XPS, and TEM, to propose a qualitative regular polyhedron model of the process.

2 Experimental

2.1 Synthesis

The synthesis of silica aerogels involves two steps: (i) the preparation of an alcogel and (ii) the solvent removal from the alcogel by ethanol supercritical drying [17]. The alcogel was prepared from tetraethoxysilane (TEOS) by a two-step method. Firstly, the designed amount of TEOS was dissolved in alcohol and then the mixture was stirred for 30 min at 35 ℃. Then, the designed amounts of water, alcohol, and catalyst were mixed and the mixture obtained was added dropwise to the TEOS solution under continuous stirring. In order to obtain alcogel with a stable structure, alcogel was submerged under alcohol for two days at room temperature. Finally, the alcogel was heated at a rate of 1 ℃/min to 300 ℃. When the temperature reached 300 ℃, the pressure was kept at 10 MPa for 2 h. This step was followed with a controlled cooling step to produce the aerogel [18].

The aerogels obtained were calcined under air atmosphere at different temperatures (400, 600, 700, 800, and 1000 ℃) to study the process of the nanoporous framework evolution, with a heating rate of 10 ℃/min. The holding time was designed as 2, 4, and 8 h.

2.2 Characterization

The phase composition of the aerogels was analyzed by powder X-ray diffraction using a D5000 apparatus (Siemens). The scanning rate was 2 (°)/min using nickel filtered Cu Kα radiation produced at 30 kV and 30 mA. The oxidation state was investigated by X-ray photoelectron spectroscopy (XPS) using a Kratos AXIS Ultra spectrometer, equipped with a monochromatic Al Kα X-ray source, a delay-line detector, and an Al anode (Al Kα = 1486.71 eV) operated at 225 W. The XPS spectra collected were analyzed using an XPSpeak software and calibrated using the adventitious O 1s peak with a fixed value of 533.3 eV. A Shirley-type background subtraction was used to fit the curve using a 20% Gaussian–80% Lorentzian function. The framework structure of the aerogels was characterized by Fourier transform infrared spectroscopy (FTIR, Iraffinity-1, Shimadzu, Japan) in the wavenumber range of 4000–400 cm^{-1}. The morphology was examined by scanning electron microscopy (SEM, Jeol, JSM-6700F). The porous framework and the nanoparticle size were characterized by transmission electron microscopy (Philips, Tecnan F20 operated at 20 kV).

N_2 adsorption isotherms were recorded with a TriStar 3000 apparatus (Quantachrome). The pore size distribution of the aerogels was obtained from the desorption branch of N_2 adsorption isotherms using Berrett–Joyner–Hallenda (BJH) method. The specific surface area was obtained by Brunauer–Emmet–Teller (BET) method.

3 Results and discussion

3.1 Effect of calcination temperature on morphology of SiO_2 aerogels

Figure 1 shows the FTIR spectra of the SiO_2 aerogels calcined at different temperatures. The asymmetric, symmetric, and rocking bending vibrations of Si–O–Si bonds are observed at 1100, 800, and 468 cm^{-1}, respectively [19,20]. The peak at 975 cm^{-1} is assigned

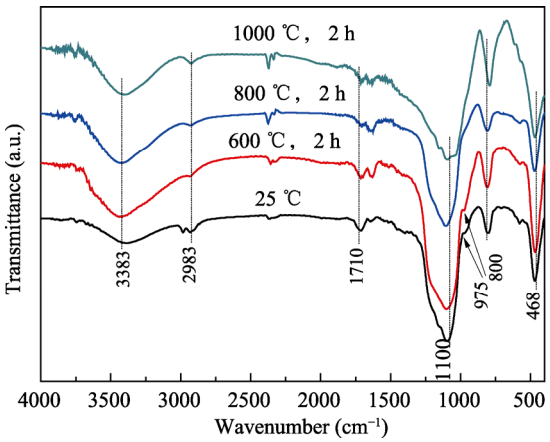

Fig. 1 FTIR spectra of SiO_2 aerogels treated at different temperatures.

to a small amount of Si–OH groups. The peak at 2983 cm^{-1} is assigned to vibrations of the CH_3 groups, suggesting the presence of Si–OC_2H_5 groups. The presence of these groups suggests an incomplete condensation during gelation process [19,21,22]. As the calcination temperature increases, the peak at 975 cm^{-1} slowly disappears and the intensity of the peak at 2983 cm^{-1} also decreases, while that of the peak at 800 cm^{-1} increases. This suggests the formation of additional Si–O–Si bonds by the condensation reaction between Si–OH and Si–OC_2H_5. The peak at 1710 cm^{-1} belongs to vibrations of water molecules [19]. Its intensity deceases with calcination temperature due to removal of water from the framework structure. Figure 2 shows a schematic view of the formation of additional Si–O–Si bonds after the thermal treatment. This process determines the morphological properties of aerogels.

Figure 3 shows O 1s XPS spectra of the as-synthesized aerogel (sample A) and three samples calcined for 2 h at 400, 600, and 800 ℃ (samples B, C, and D, respectively). The binding energy (BE) and the fraction (mol%) of different elements are listed in Table 1. This estimation was obtained from the deconvolution of the corresponding XPS bands following the method described in Refs. [23,24]. The peak at 533.18–533.50 eV originates from the Si–O–Si groups [25,26], the peak at 532.62–532.93 eV originates from the Si–OH groups [27], while the peak at 532.31–532.46 eV originates from the Si–OC_2H_5 groups [28]. As the calcination temperature increases, the amount of Si–O–Si groups increases from 51.8% to 96.6%, while that of Si–OH and Si–OC_2H_5 groups decreases, indicating the formation of additional bonds of Si–O–Si via the condensation reaction, in agreement with the results obtained from the FTIR study. The formation of the additional bonds of Si–O–Si results in the shrinkage of the aerogel framework structure. This process is responsible for an increase of the total pore volume and the specific surface area. The Si–OH groups disappear at 800 ℃ while the amount of Si–OC_2H_5 groups decreases to 3.1% , suggesting that the framework is preferentially formed by the Si–O–Si bonds.

Figure 4 shows the XRD patterns of four SiO_2 aerogels calcined at different temperatures. Wide peaks are observed in all samples indicating an amorphous structure. The intensity of the main peak increases with the calcination temperature which confirms ongoing crystallization process.

Table 2 shows the specific surface area, pore volume, and pore size of the as-synthesized aerogels and those thermally treated. Additionally, curves of specific surface area and average pore diameter of the SiO_2 aerogels obtained from different conditions are shown in Fig. 5.

It can be seen in Table 2 that the surface area of

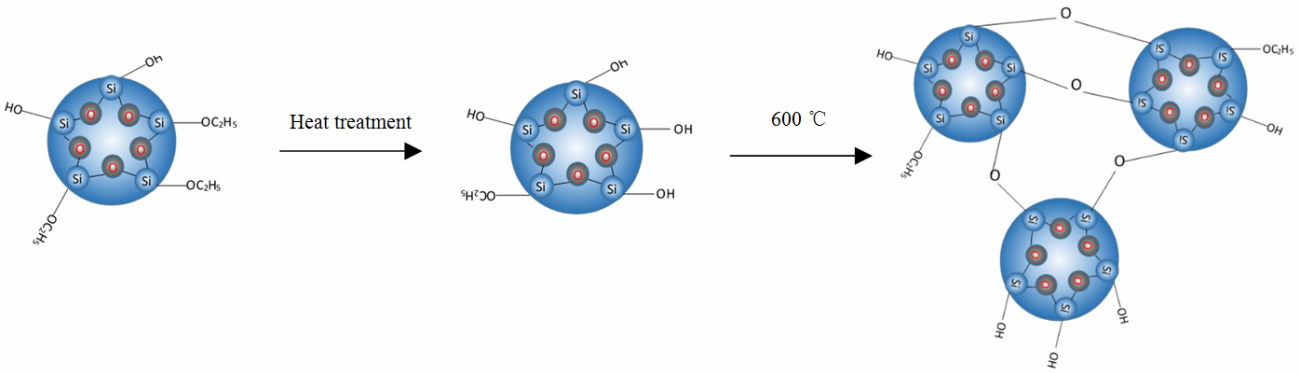

Fig. 2 Schematic view of the formation of additional Si–O–Si bonds in aerogels after a thermal treatment.

SiO_2 aerogels increases initially and then decreases with increasing calcination temperature. It reaches a maximum value of 883 m^2/g at 600 ℃. The pore diameter monotonously decreases due to the formation of additional bonds of Si–O–Si formed via condensation reaction between the silanol group and the remaining Si–OC_2H_5 on the secondary particles [29], as it is also confirmed by the FTIR and XPS studies. Additional pores are formed between the aerogel clusters. The framework structure shrinks due to the formation of the new bonds. This process is responsible for the increase of the specific surface area and it reduces the average pore diameter. The largest particle size increases and the shrinkage of the framework occurs at the highest calcination temperature. This reduces both

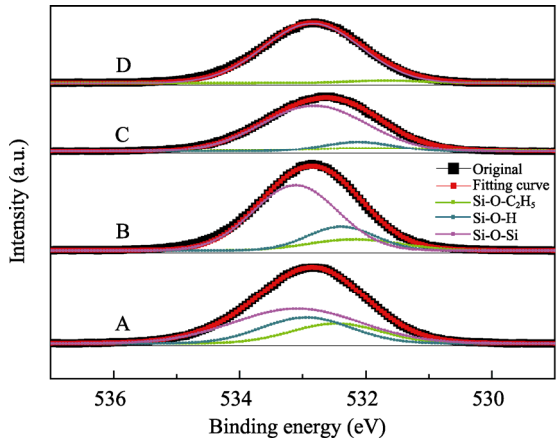

Fig. 3 O 1s XPS spectra of aerogels treated at different temperatures: (A) as-synthesized; (B) 400 ℃, 2 h; (C) 600 ℃, 2 h; (D) 800 ℃, 2 h.

Table 1 Quantitative O 1s XPS analysis of SiO_2 aerogels calcined at different temperatures

Sample / Orbital	Binding energy (eV)/atomic percentage (%)			
	A	B	C	D
Si–O–Si	533.18/51.82	533.31/67.25	533.31/80.67	533.50/96.85
Si–OH	532.93/27.29	532.58/19.89	532.62/11.21	—
Si–OC_2H_5	532.46/20.89	532.37/12.55	532.31/8.12	532.32/3.14

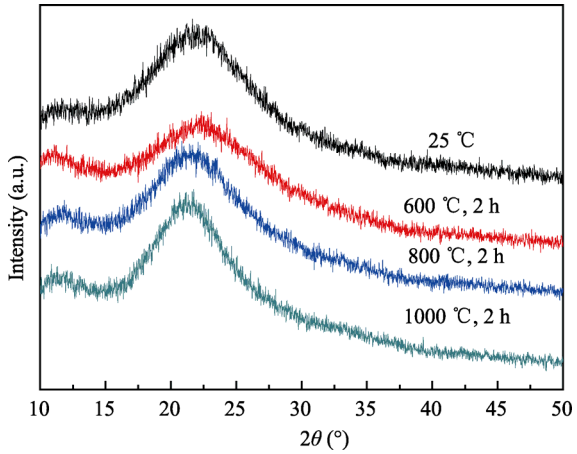

Fig. 4 XRD patterns of SiO_2 aerogels calcined at different temperatures.

Table 2 BET, pore volume, and pore size values of SiO_2 aerogels before and after thermal treatment at different temperatures

Heat treatment	Surface area (m^2/g)	Average pore diameter (nm)	Pore volume (cm^3/g)
Room temperature	635	22.2	4.53
600 ℃, 2 h	883	14.7	3.45
600 ℃, 4 h	638	6.7	2.04
600 ℃, 8 h	600	11.5	2.28
800 ℃, 2 h	727	7.9	1.64
800 ℃, 4 h	299	17.6	1.23
800 ℃, 8 h	224	11.6	1.01
1000 ℃, 2 h	2.06	3.1	0.005
1000 ℃, 4 h	0.61	1.4	0.07
1000 ℃, 8 h	2.07	0.3	0.01

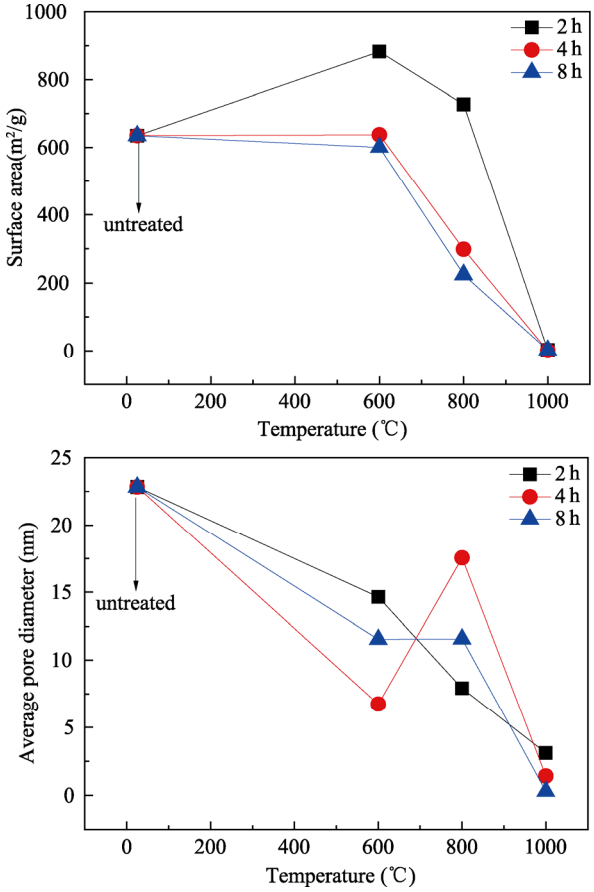

Fig. 5 Specific surface area and average pore diameter of SiO_2 aerogels treated at different temperatures.

the surface area and the average pore diameter. The surface area of aerogels decreases dramatically after a long exposure to high temperature due to the continuous framework shrinkage of the SiO_2 aerogels.

Figure 6 shows typical N_2 adsorption/desorption isotherms and the corresponding pore size distribution (PSD) plots of the aerogels before and after thermal treatment. The PSD plots were obtained from the desorption branch of N_2 isotherms by the BJH method. The presence of hysteresis loop is due to the capillary condensation occurred in the mesoporous [31]. The nitrogen adsorption follows type-IV isotherm indicating that a rather high amount of mesopores is present in the structure of SiO_2 aerogel [30]. The number of mesoporous decreases at higher temperatures due to the accumulation of larger secondary particles. The average mesopore size of the as-synthesized aerogels is in the range of 20–40 nm. The SiO_2 aerogel treated at 600 ℃ for 2 h has a broader PSD with an average diameter of 14.7 nm. After the thermal treatment for 4 h, the mean pore size shifts to a lower value (6.7 nm). The PSD becomes more uniform, which can be caused by a complete transformation of the remaining $Si–OC_2H_5$ groups to Si–OH groups by oxidation [32]. However, the samples calcined for 8 h have a wider PSD than those calcined for 4 and 2 h. The latter could be due to the fact that the framework shrinks and the particles grow even after a time period of 4 h. This plays an important role in the stabilization of the porous framework. A surface area of 727 m^2/g and an average pore diameter of 7.9 nm were observed after the treatment at 800 ℃ for 2 h, The number of pores reduces and the pore size distribution becomes non-uniform. Moreover, the surface area reduces dramatically after the treatments with a duration of more than 4 h. This reveals that the particles keep growing and the framework finally collapses. A further increase in the temperature to 1000 ℃ results in a complete collapse of porous structure. The samples transform to a semitransparent glass with little porosity [33].

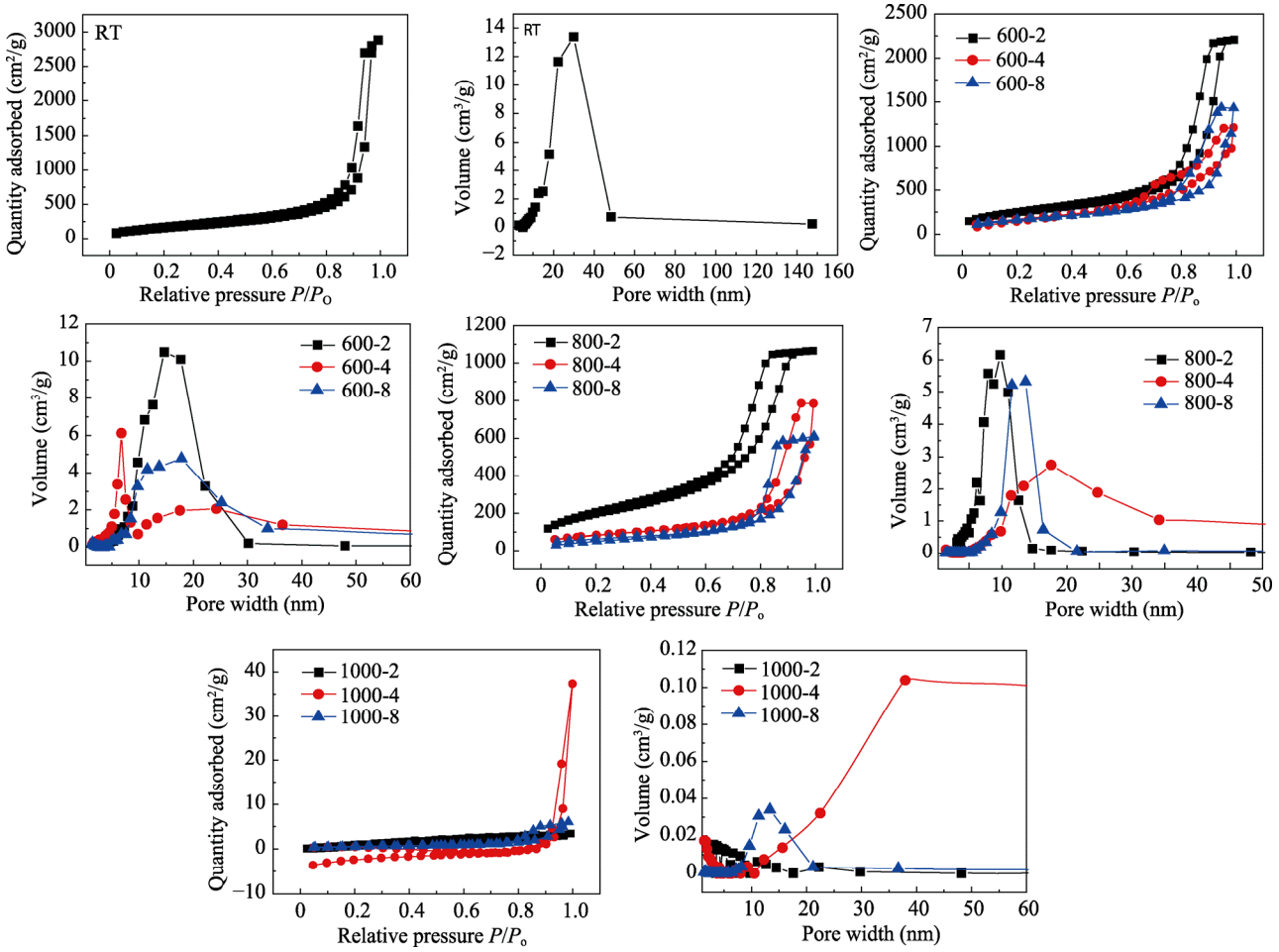

Fig. 6 N_2 adsorption/desorption isotherms and the PSD of SiO_2 aerogels before and after thermal treatment.

3. 2 Morphology and microstructure of SiO_2 aerogels

Figure 7 presents typical SEM photographs of SiO_2 aerogels before and after the thermal treatment. It can be seen that the secondary particles are aggregated and condensed to form clusters. The crosslinking among these clusters generates a porous framework. As the temperature increases, the amount of mesopores first increases (in Fig. 7(b)) and then decreases (in Figs. 7(c) and 7(d)). The morphology of the porous framework in aerogels changes from loose (in Fig. 7(a)) to compact (in Fig. 7(b)), and then dense (in Fig. 7(c)). Finally the formation of larger particles results in a collapse of porous structure (in Fig. 7(d)). It can also be seen that the pore shape changes from a tetrahedron to an octahedron.

Figure 8 shows TEM images of the SiO_2 aerogels calcined at different temperatures. All samples show a randomly interconnected framework, which is composed of irregular spherical nanoparticles. As it can be seen in Figs. 8(a), 8(b), and 8(c), the particle size of these samples ranges between 5 and 10 nm, while much bigger particles of 40–50 nm are observed at 1000 ℃ (Fig. 8(d)). This indicates that the neck growth results in the collapse of the tunnel structure above 800 ℃.

3. 3 Nanoporous framework evolution of SiO_2 aerogels calcined at different temperatures

No literature reports on the evolution of mesoporous framework of the aerogels during the calcination process. However, the understanding of this process is important for prediction of the morphology and the thermal stability of the aerogels. According to the electrostatic valence rule, the cells of SiO_2 aerogel possess [SiO_4] tetrahedron structure, and vertexes of this structure are occupied by the same structure. Being connected together, they form a three-dimensional network structure, a spherical granular-secondary particle [34]. These secondary particles connect with each other to form the polyhedron-nanoporous framework.

Thus, we assume that the microstructure of the aerogel is composed of different regular polyhedrons, and the pore size is controlled by the diameter of face inscribed circle. In turn, the pore volume equals to the

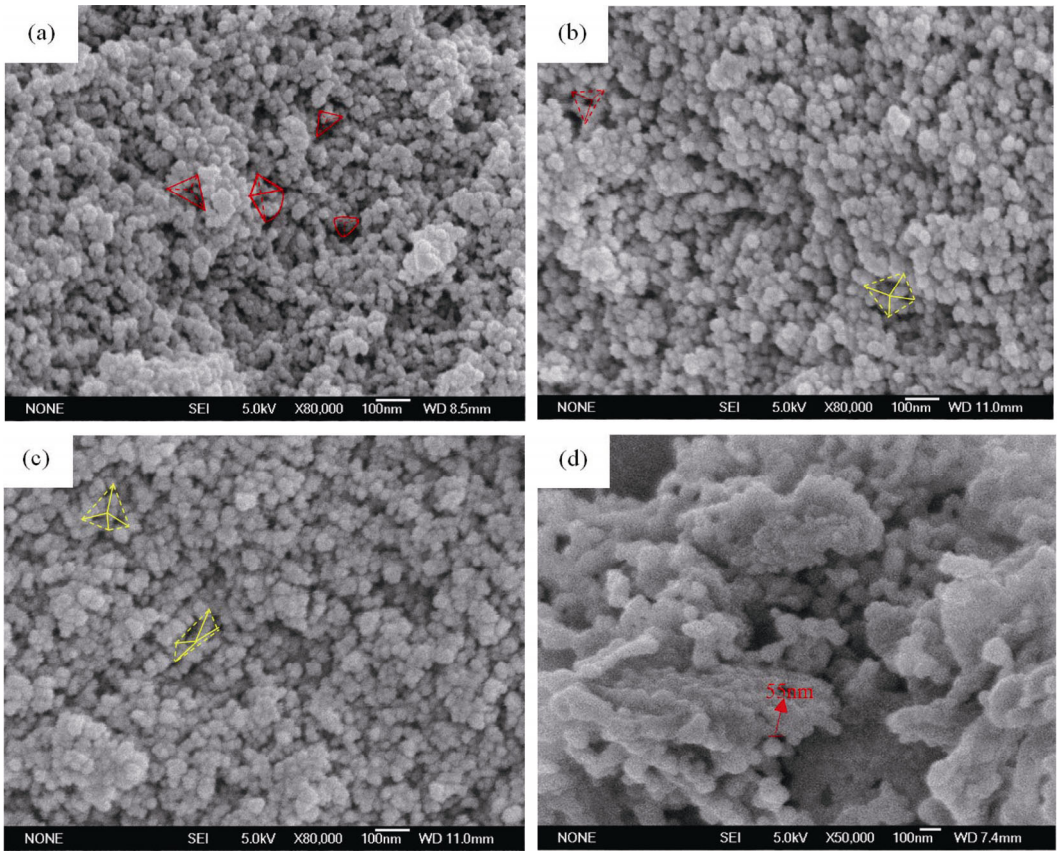

Fig. 7 SEM images of SiO_2 aerogels calcined at different temperatures: (a) room temperature; (b) 600 ℃, 2 h; (c) 800 ℃, 2 h; (d) 1000 ℃, 2 h. Graphics in red stand for tetrahedron, yellow for octahedron.

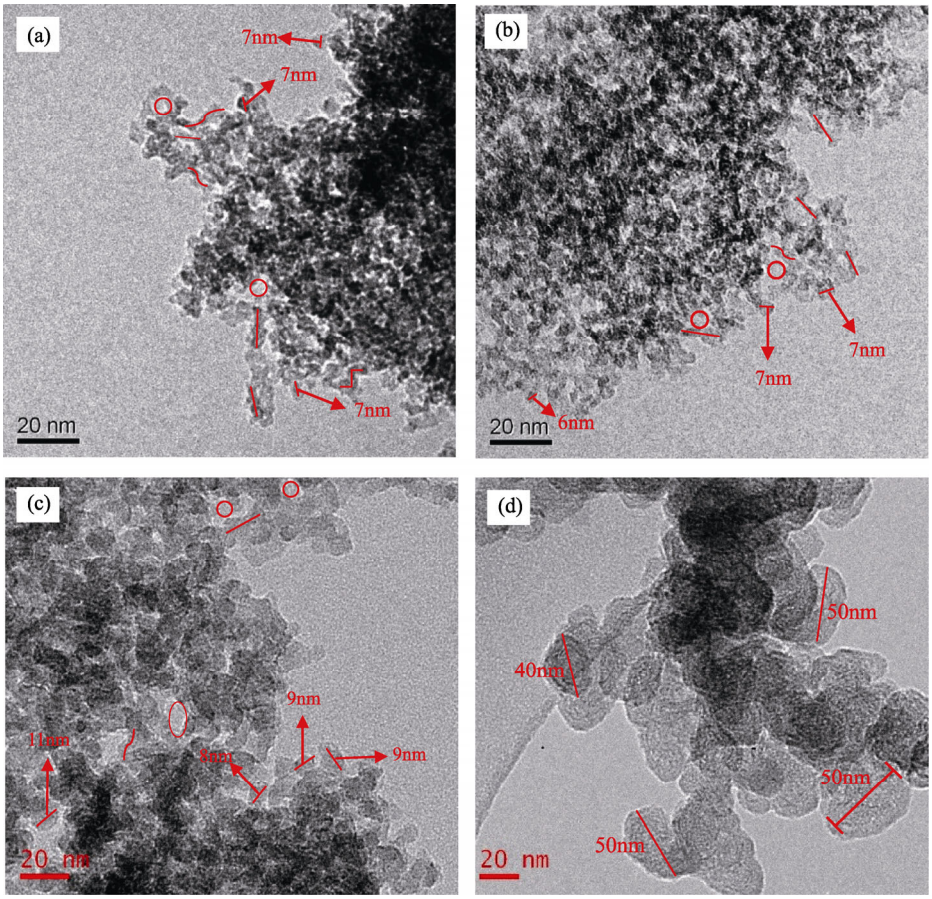

Fig. 8 TEM images of SiO_2 aerogels calcined at different temperatures: (a) room temperature; (b) 600 ℃, 2 h; (c) 800 ℃, 2 h; (d) 1000 ℃, 2 h; symbols of circle stand for pores and line for framework.

sum of individual polyhedron volumes. The following equations are used to estimate the key parameters of the mesoporous framework evolution.

Firstly, the weight of each secondary particle is calculated by Eq. (1):

$$m = \frac{4}{3}\pi \times \left(\frac{d}{2}\right)^3 \times \rho_{\text{aerogel}} \tag{1}$$

The number of secondary particles is calculated by Eq. (2):

$$N = \frac{M}{m} = \frac{6M}{\pi d^3 \rho_{\text{aerogel}}} \tag{2}$$

where m is the weight of secondary particles, d is its diameter (nm) (taken from TEM images), M is the sample weigth, and ρ_{aerogel} is the apparent density of the silica aerogel (2.1 g/cm^3) [35].

The number of particles on each edge of polyhedron (remove both ends) is calculated by Eq. (3):

$$m = \frac{a-d}{d} \tag{3}$$

The total number of particles of each regular polyhedron is calculated by Eq. (4):

$$p = e \times \beta + m \times h \times \frac{\theta}{2\pi} \tag{4}$$

The number of regular polyhedron is calculated by Eq. (5):

$$n = \frac{N}{p} \tag{5}$$

Combining Eqs. (1), (2), (3), (4), and (5), the total volume of polyhedrons in the aerogel can be calculated by Eq. (6):

$$V = \frac{12M}{d^2 \rho_{\text{aerogel}} \left[2e\pi d\beta + h\theta(a-d)\right]} \times V_{\text{regular-polyhedron}} \tag{6}$$

where a represents the polyhedron edge length, β is the space volume percentage occupied by vertex, h is the number of edge of regular polyhedron, e is the vertex number, and θ is the dihedral angle. The estimated framework and calculated pore volume of SiO_2 aerogels are listed in Table 3. The calculated results are

Table 3 Estimated porous framework and calculated pore volume of SiO_2 aerogels treated at different temperatures

Heat treated conditions	Room temperature	600 ℃, 2 h		700 ℃, 2 h		800 ℃, 2 h	1000 ℃, 2 h
Desorption pore volume (cm^3)	0.2065	0.2021		0.1016		0.0531	0.0052
Regular polyhedron type	Tetrahedron	Tetrahedron	Octahedron	Tetrahedron	Octahedron	Octahedron	—
Total polyhedral volume (cm^3)	0.2402	0.1704	0.2282	0.0815	0.1101	0.0545	2.3×10^{-3}
Estimated nanoporous framework	Total tetrahedron	Tetrahedron:octahedron = 1:1		Tetrahedron:octahedron = 1:2		Total octahedron	Densification
Calculated pore volume (cm^3)	0.2402	0.1993		0.1005		0.0545	—

compared with the corresponding experimental data.

It can be seen in Table 3 that the calculated values of pore volume are in good agreement with the experimental results. The porous framework of as-synthesized samples consists of tetrahedrons and that calcined at 1000 ℃ of octahedrons. A tetrahedron to octahedron ratio of 1 is observed in samples calcined at 600 ℃, while this ratio decreases to 0.5 after calcination at 800 ℃.

Figure 9 presents a schematic evolution of SiO_2 aerogel framework as a function of calcination temperature. Figure 10 shows further geometrical interpretation of the model proposed. As for SiO_2 aerogels at room temperature in Fig. 9, the nanoporous framework totally is composed of tetrahedron with a pore size of about 22.28 nm; as the temperature reaches to 600 ℃, the framework is composed of tetrahedron and octahedron with a ratio of 1:1. It becomes more compact, being due to the formation of extra Si–O–Si bond via the condensation reaction between Si–OH and/or Si–OC_2H_5 on the secondary particles, as shown in Fig. 2, and it is also consistent with the SEM (Fig. 6(b)). When the temperature reaches to 700 ℃, the quantity ratio of tetrahedron and octahedron reaches up to 1:2. The pore size of aerogel is 11.04 nm at 700 ℃. With the heat treatment temperature increases to 800 ℃, the nanoporous framework totally is composed of octahedron with a pore size of about 7.91 nm. In addition, the newly formed Si–O–Si bonds can produce a shrinkage of nanoporous framework and result in a decrease of pore size. A high local stress and the liquid in the pores between the particles result in the deformation of individual particles. This process can eventually cause a rearrangement of particles during the thermal treatment process [36]. Above 600 ℃, the newly formed Si–O–Si bonds and the rearrangement of particles result in a variety of pore shapes and particles sizes. The aerogels are stabilized by reducing the surface energy via the pore collapse and particle growth after the treatment at 1000 ℃, as shown in Fig. 7(d).

In reality, the geometric figure shown in Fig. 9 should be a twisted shape as the silica aerogels mainly consist of Si–O–Si groups whose bond angle is 109°28′. Due to the calculation requirement, the model was described by tetrahedron and octahedron.

4 Conclusions

(1) SiO_2 aerogels treated at different temperatures and holding time all possess amorphous structure; with the increase of treated temperatures, it has an obvious trend of crystallization.

(2) With the increase of treated temperatures, BET values of SiO_2 aerogels increase initially and then decrease; it reaches maximum value of 882.81 m^2/g when treated at 600 ℃ for 2 h, while the values of average pore diameter simply decrease. These varieties may be due to the newly formed Si–O–Si bonds via condensation reaction between the secondary particles during heat treatment process; it can not only add the amount of nanopores but also help to shrink the skeleton; the former can improve the BET values and the latter helps to reduce the average pore diameter of aerogels. A higher temperature may result in the skeleton transformation and particle size growth; both factors lead to the reduction of BET and average pore diameter values.

(3) Nanoporous skeleton of SiO_2 aerogels at room temperatures is mainly composed of tetrahedron with a pore size of about 22.28 nm, and when treated at 600 ℃, its microstructure is mainly composed of tetrahedron and octahedron with a ratio of 1:1 and the relative pore size is about 14.65 nm. A higher temperature results in an increase of octahedron amount in the nanoporous framework and a decrease of the pore size in aerogels. Finally, treating at 1000 ℃ results in an approximate dense SiO_2 bulk via the framework collapse and particle growth. The newly formed Si–O–Si bonds, the high local stress, and liquid

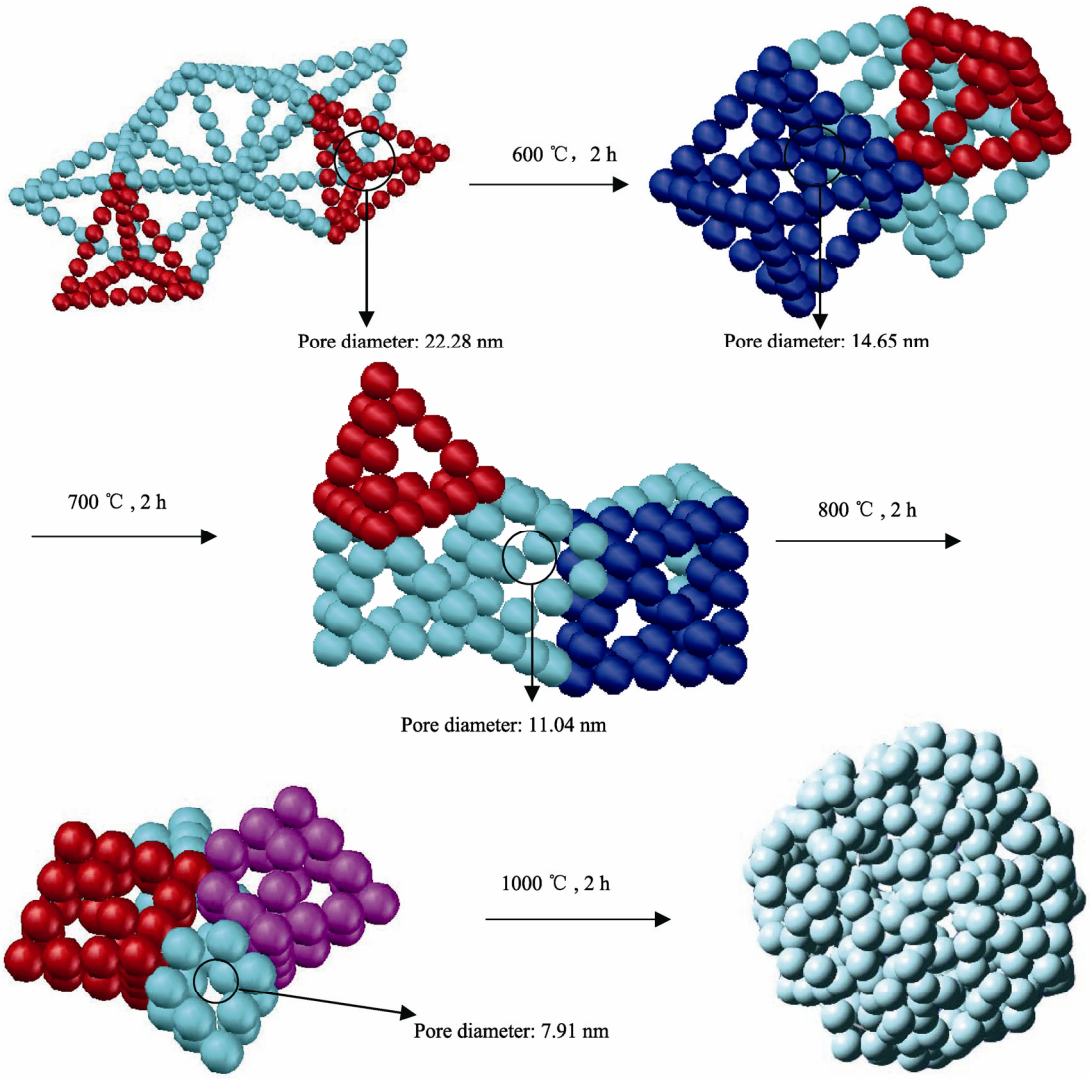

Fig. 9 Models of the transformation mechanism of pore structure during heat treatment.

Fig. 10 Additional interpretation of geometric model.

phase between particles can cause the particle growth and rearrangement of nanoporous framework.

References

[1] Gao QF. Nano-porous silica, alumina aerogels and thermal super-insulation composites. Ph.D. Thesis. Changsha, China: National University of Defense Technology, 2009. (in Chinese)

[2] Rueda M, Sanz-Moral LM, Nieto-Márquez A, *et al.* Production of silica aerogel microparticles loaded with ammonia borane by batch and semicontinuous supercritical drying techniques. *J Supercrit Fluid* 2014, **92**: 299–310.

[3] Lu G, Wang X-D, Duan Y-Y, *et al.* Effects of non-ideal structures and high temperatures on the insulation properties of aerogel-based composite materials. *J Non-Cryst Solids* 2011, **357**: 3822–3839.

[4] Li M, Jiang H, Xu D, *et al.* Low density and hydrophobic silica aerogels dried under ambient pressure using a new co-precursor method. *J Non-Cryst Solids* 2016, **452**:

187–193.
[5] Tang X, Sun A, Chu C, *et al.* A novel silica nanowire-silica composite aerogels dried at ambient pressure. *Mater Design* 2017, **115**: 415–421.
[6] Li XW, Duan YY, Wang XD. Impacts of structural changes of SiO_2 aerogel under high temperature on its insulation performance. *J Therm Sci Tech* 2011, **10**: 189–193.
[7] Maleki H, Durães L, Portugal A. A new trend for development of mechanical robust hybrid silica aerogels. *Mater Lett* 2016, **179**: 206–209.
[8] Lu Z, Yuan Z, Liu Q, *et al.* Multi-scale simulation of the tensile properties of fiber-reinforced silica aerogel composites. *Mat Sci Eng A* 2015, **625**: 278–287.
[9] Kim C-Y, Lee J-K, Kim B-I. Synthesis and pore analysis of aerogel-glass fiber composites by ambient drying method. *Colloid Surf A* 2008, **313–314**: 179–182.
[10] Wu H, Liao Y, Ding Y, *et al.* Engineering thermal and mechanical properties of multilayer aligned fiber-reinforced aerogel composites. *Heat Transfer Eng* 2014, **35**: 1061–1070.
[11] Fenech J, Viazzi C, Bonino J-P, *et al.* Morphology and structure of YSZ powders: Comparison between xerogel and aerogel. *Ceram Int* 2009, **35**: 3427–3433.
[12] Reichenauer G, Heinemann U, Ebert H-P. Relationship between pore size and the gas pressure dependence of the gaseous thermal conductivity. *Colloid Surf A* 2007, **300**: 204–210.
[13] Zhou CL, Yang J, Sui XY, *et al.* Impacts of structural change of SiO_2 aerogel under different time and high temperature conditions on insulation performance. *Adv Ceram* 2014, **5**: 11–16.
[14] Huang D, Guo C, Zhang M, *et al.* Characteristics of nanoporous silica aerogel under high temperature from 950 ℃ to 1200 ℃. *Mater Design* 2017, **129**: 82–90.
[15] Olivi-Tran N, Jullien R. Numerical simulations of aerogel sintering. *Phys Rev B* 1995, **52**: 258.
[16] Chu P, Liu H, Li Y, *et al.* Syntheses of SiC–TiO_2 hybird aerogel via supercritical drying combined PDCs route. *Ceram Int* 2016, **42**: 17053–17058.
[17] Rao AV, Hegde ND, Hirashima H. Absorption and desorption of organic liquids in elastic superhydrophobic silica aerogels. *J Colloid Interface Sci* 2007, **305**: 124–132.
[18] Zhang Z, Scherer GW. Supercritical drying of cementitious materials. *Cement Concrete Res* 2017, **99**: 137–154.
[19] Shao Z, Luo F, Cheng X, *et al.* Superhydrophobic sodium silicate based silica aerogel prepared by ambient pressure drying. *Mater Chem Phys* 2013, **141**: 570–575.
[20] Saeed S, Soubaihi RMA, White LS, *et al.* Rapid fabrication of cross-linked silica aerogel by laser induced gelation. *Microporous Mesoporous Mater* 2016, **221**: 245–252.
[21] García-Torres BA, Aguilar-Elguezabal A, Román-Aguirre M, *et al.* Synthesis of silica aerogels microspheres prepared by ink jet printing and dried at ambient pressure without surface hydrophobization. *Mater Chem Phys* 2016, **172**: 32–38.
[22] Shahzamain M, Bagheri R, Masoomi M. Synthesis of silica-polybutadiene hybrid aerogel: The effects of reaction conditions on physical and mechanical properties. *J Non-Cryst Solids* 2016, **452**: 325–335.
[23] Sutka A, Pärna R, Mezinskis G, *et al.* Effects of Co ion addition and annealing conditions on nickel ferrite gas response. *Sensor Actuat B: Chem* 2014, **192**: 173–180.
[24] Barba A, Clausell C, Nuño L, *et al.* ZnO and CuO crystal precipitation in sintering Cu-doped Ni–Zn ferrites. II. Influence of sintering temperature and sintering time. *J Eur Ceram Soc* 2017, **37**: 169–177.
[25] Nocun M, Cholewa-Kowalska K, Łączka M. Structure of hybrids based on TEOS-cyclic forms of siloxane system. *J Mol Struct* 2009, **938**: 24–28.
[26] Wang H, Wu Q, Cao D, *et al.* Synthesis of SnSb-embedded carbon–silica fibers via electrospinning: Effect of TEOS on structural evolutions and electrochemical properties. *Mater Today* 2016, **1–2**: 24–32.
[27] Yang J, Chen J. Surface free energy and surface structure of methyl-modified silica membranes. *J Mater Eng* 2008, **10**: 177–182.
[28] Kim N-H, Ko P-J, Seo Y-J, *et al.* Improvement of TEOS-chemical mechanical polishing performance by control of slurry temperature. *Microelectron Eng* 2006, **83**: 286–292.
[29] Li Z, Gong L, Li C, *et al.* Silica aerogel/aramid pulp composites with improved mechanical and thermal properties. *J Non-Cryst Solids* 2016, **454**: 1–7.
[30] He S, Huang D, Bi H, *et al.* Synthesis and characterization of silica aerogels dried under ambient pressure bed on water glass. *J Non-Cryst Solids* 2015, **410**: 58–64.
[31] Sing KSW, Williams RT. Physisorption hysteresis loops and the characterization of nanoporous materials. *Adsorpt Sci Technol* 2004, **22**: 773–782.
[32] Shi C, Zhang S, Jiang Y, *et al.* High temperature properties of silica aerogel. *Rare Metal Mat Eng* 2016, **45**: 210–213.
[33] Wagh PB, Pajonk GM, Haranath D, *et al.* Influence of temperature on the physical properties of citric acid catalyzed TEOS silica aerogels. *Mater Chem Phys* 1997, **50**: 76–81.
[34] Li Z-H, Gong Y-J, Pu M, *et al.* Determination of structure of SiO_2 colloidal particle by SAXS. *Chin J Inorg Chem* 2003, **19**: 252–256.
[35] Morales-Flórez V, Rosa-Fox NDL, Piñero M, *et al.* The cluster model: A simulation of the aerogel structure as a hierarchically-ordered arrangement of randomly packed spheres. *J Sol-Gel Sci Technol* 2005, **35**: 203–210.
[36] Kuczynski GC. *Sintering Processes*. Now York, 1979.

Open Access The articles published in this journal are distributed under the terms of the Creative Commons Attribution 4.0 International License (http://creativecommons.org/licenses/by/4.0/), which permits unrestricted use, distribution, and reproduction in any medium, provided you give appropriate credit to the original author(s) and the source, provide a link to the Creative Commons license, and indicate if changes were made.